JCI The Journal of Clinical Investigation

# Germline RUNX1 variation and predisposition to childhood acute lymphoblastic leukemia

Yizhen Li, … , Mignon L. Loh, Jun J. Yang

*J Clin Invest.* 2021. https://doi.org/10.1172/JCI147898.

Research In-Press Preview Genetics Oncology

## Graphical abstract

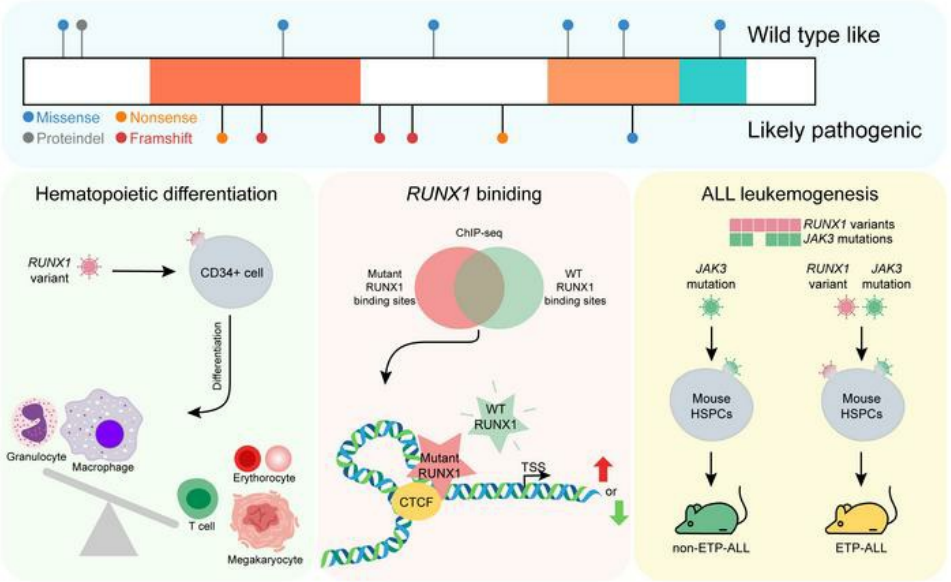


## Find the latest version:

https://jci.me/147898/pdf

# Germline *RUNX1* Variation and Predisposition to Childhood Acute Lymphoblastic Leukemia

Yizhen Li, PhD[1*] , Wentao Yang, PhD[1*], Meenakshi Devidas, PhD[2], Stuart S. Winter, MD[3], Chimene Kesserwan, MD[4], Wenjian Yang, PhD[1], Kimberly P. Dunsmore, MD[5], Colton Smith, PhD[1], Maoxiang Qian, PhD[6], Xujie Zhao, MS[1], Ranran Zhang, MS[1], Julie M. Gastier-Foster, PhD[7], Elizabeth A. Raetz, MD[8], William L. Carroll, MD[8], Chunliang Li, PhD[9], Paul P. Liu[10], Karen R. Rabin, MD, PhD[11], Takaomi Sanda[12,13], Charles G. Mullighan, MBBS, MD[14], Kim E. Nichols, MD[15], William E. Evans, PharmD[1,16], Ching-Hon Pui, MD[15,16], Stephen P. Hunger, MD[17], David T. Teachey[18], MD, Mary V. Relling, PharmD[1,16], Mignon L. Loh, MD[19], Jun J. Yang, PhD[1, 15, 16, #]

*[1]Department of Pharmaceutical Sciences, St. Jude Children's Research Hospital, Memphis, TN, [2]Department of Global Pediatric Medicine, St. Jude Children's Research Hospital, Memphis, TN, [3]Children's Minnesota Research Institute, Children's Minnesota, Minneapolis, MN, [4]Center for Cancer Research, Genetics Branch, National Cancer Institute, USA, [5]Children's Hematology and Oncology, Carilion Clinic and Virginia Tech Carilion School of Medicine, Roanoke, VA, [6]Children's Hospital and Institutes of Biomedical Sciences, Fudan University, Shanghai, China, [7]Baylor College of Medicine and Texas Children's Hospital, Houston, TX, [8]Division of Pediatric Hematology and Oncology, Perlmutter Cancer Center, New York University Langone Health, New York, [9]Tumor Cell Biology, St. Jude Children's Research Hospital, Memphis, TN, [10]Oncogenesis and Development Section, National Human Genome Research Institute, National Institutes of Health, Bethesda, MD, USA, [11]Texas Children's Cancer and Hematology Centers, Baylor College of Medicine, Houston, TX, [12]Cancer Science Institute of Singapore, National University of Singapore, Singapore, [13]Department of Medicine, Yong Loo Lin School of Medicine, National University of Singapore, Singapore, [14]Department of Pathology, St. Jude Children's Research Hospital, Memphis, TN, [15]Department of Oncology, St. Jude Children's Research Hospital, Memphis, TN, [16]Hematological Malignancies Program, St. Jude Children's Research Hospital, Memphis, TN, [17]Department of Pediatrics and Center for Childhood Cancer Research, Children's Hospital of Philadelphia and the Perelman School of Medicine at the University of Pennsylvania, Philadelphia, PA, [18]Division of Oncology, Department of Pediatrics, Center for Childhood Cancer Research, Children's Hospital of Philadelphia and Perelman School of Medicine, University of Pennsylvania, Philadelphia, PA, [19]Department of Pediatrics, Benioff Children's Hospital and the Helen Diller Family Comprehensive Cancer Center, University of California San Francisco, San Francisco, CA*

*These authors contribute equally.

**[#] Corresponding author**: Jun J Yang, 262 Danny Thomas Place, MS313, Memphis, TN, 38105; 901-595-2517; jun.yang@stjude.org

**Conflict of interest:** The authors have no conflict of interest to declare.

**Abstract**

Genetic alterations in the *RUNX1* gene are associated with benign and malignant blood disorders, particularly of megakaryocyte and myeloid lineages. The role of RUNX1 in acute lymphoblastic leukemia (ALL) is less clear, particularly how germline genetic variation influences the predisposition to this type of leukemia. Sequencing 4,836 children with B-ALL and 1,354 cases of T-ALL, we identified 31 and 18 germline *RUNX1* variants, respectively. *RUNX1* variants in B-ALL consistently showed minimal damaging effects. By contrast, 6 T-ALL-related variants result in drastic loss of RUNX1 activity as a transcription activator *in vitro*. Ectopic expression of dominant-negative *RUNX1* variants in human CD34+ cells repressed differentiation into erythroid, megakaryocytes, and T cells, while promoting myeloid cell development. Chromatin immunoprecipitation sequencing of T-ALL models showed distinctive patterns of RUNX1 binding by variant proteins. Further whole genome sequencing identified *JAK3* mutation as the most frequent somatic genomic abnormality in T-ALL with germline *RUNX1* variants. Co-introduction of *RUNX1* variant and *JAK3* mutation in hematopoietic stem and progenitor cells in mice gave rise to T-ALL with early T-cell precursor phenotype. Taken together, these results indicated that *RUNX1* is an important predisposition gene for T-ALL and pointed to novel biology of RUNX1-mediated leukemogenesis in the lymphoid lineages.

## Introduction

Acute lymphoid leukemia (ALL) is the most common cancer in children. The exact cause of ALL is incompletely understood, although somatic genomic abnormalities are well documented affecting a wide range of signaling pathways(1). There is also growing evidence of inherited susceptibility to ALL. For example, common genetic polymorphisms in genes such as *IKZF1*(2), *ARID5B* (3), *CDKN2A*(4), *GATA3* (5, 6), *CEBPE*(7), *PIP4K2A*(8), and *TCF3-PBX1*(9) are associated with the risk of ALL in an age- and subtype-dependent manner. On the other hand, rare germline variants have been linked to familial predisposition to childhood ALL, particularly notable in *TP53*(10)*, ETV6*(11)*,* and *IKZF1*(2, 9)*.* These findings point to a strong genetic basis of inter-individual variability in ALL risk.

The RUNX1 protein plays key roles in definitive hematopoiesis (12). RUNX1 functions as a transcription factor by forming a heterodimer with core binding factor β (CBFβ). RUNX1 consists of a Runt homology domain (RHD) responsible for DNA binding and cofactor interaction (13) and the C-terminal transcriptional activation domain (TAD) that recruits co-activators and activates the expression of RUNX1 target genes (14). *RUNX1* germline variants are associated with familial platelet disorder (FPD). Many patients with FPD develop leukemia later in life, predominately acute myeloid leukemia (AML) and myelodysplastic syndrome (MDS) (15-18). Somatic *RUNX1* mutations are also recurrent in B- and T-ALL; they mostly occur in the RHD and TAD domains and more common in T-ALL(19, 20). *RUNX1* mutations also are related to poor prognosis in T-ALL(19) and particularly enriched in those with early T-cell precursor immunophenotype (ETP)(21). The role of germline *RUNX1* variants in the pathogenesis of ALL is much less known, and their pattern, prevalence, and functional consequences in this lymphoid malignancy have not been comprehensively investigated.

Here we report results from targeted germline sequencing of 6,190 children with B- or T-ALL enrolled in frontline Children's Oncology Group (COG) and St. Jude Children's Research Hospital (St. Jude) ALL trials. We observed a lineage-specific pattern of germline variation in the *RUNX1*

gene, with deleterious variants exclusively present in T-ALL patients. Furthermore, we experimentally characterized *RUNX1* variants for their effects on transcription factor activity, subcellular localization, cofactor interaction, *in vitro* hematopoiesis, and genome wide RUNX1 binding profile. Finally, we examined the somatic genomic landscape of T-ALL arising from *RUNX1* germline variants and modeled *RUNX1*-mediated leukemogenesis in mouse models.

## Results

### Identification of germline *RUNX1* variants in pediatric ALL

To comprehensively characterize inherited *RUNX1* variations in ALL, we performed targeted sequencing in germline DNA of 4,836 patients with newly diagnosed B-ALL and 1,354 patients with T-ALL enrolled on COG and St. Jude frontline trials (**Figure 1A and Table 1**). We identified 31 unique variants in 61 B-ALL cases and 18 unique variants in 26 T-ALL cases. Seven of these variants were found in both B- and T-ALL (**Figure 1A and Table 1**).

Of the 31 variants in B-ALL, 6 were not observed in the general population (Genome Aggregation database, gnomAD, n = 15,496), 18 were rare with a maximum allele frequency of 0.00122%, and the remaining 7 were considered common variants with allele frequency > 0.01% (**Figure 1A and Table 1**). All variants in B-ALL except one were missense, most of which were in the C-terminus distal to the DNA binding runt-homology domain (RHD, **Figure 1B**). Of the 18 variants in T-ALL cases, 8 were absent in the gnomAD dataset, 5 were rare with a maximum allele frequency of 0.00239%, and the remaining 5 were common variants (**Figure 1A and Table 1**). Five of T-ALL-related variants were frameshift or nonsense, including 1) p.K117* and p.S141fs which truncated both the RHD and the transcription activation domain (TAD, **Figures 1B and S1**) and 2) p.Q213fs, p.R232fs, and p.Y287* that resulted in the loss of TAD only (**Figure S1**). Seven missense and 1 in-frame deletion variants in T-ALL were distributed across *RUNX1*. This is significantly different from the pattern of missense *RUNX1* variants in FPD with associated myeloid malignancy (FPDMM) (**Figure 1C**)(22), which are largely restricted to the DNA-binding domain (p-value = $8.35 \times 10^{-5}$, Fisher's exact test).

### Effects of *RUNX1* variants on transcriptional regulation, cellular localization, and protein-protein interaction

To understand how germline *RUNX1* variants affect gene function, we first examined their transcription activator activity using the luciferase reporter assay in Hela cells. With *SPI1* as the

RUNX1 target gene (23), none of the germline variants identified in B-ALL showed a significant impact on reporter gene transcription compared to the wildtype (WT) protein and therefore were not studied further (**Figure 2A and S1A**). Among *RUNX1* alleles seen in T-ALL, all frameshift and nonsense variants (p.K117*, p.S141fs, p.S213fs, p.R232fs, and p.Y287*) and also missense variant G365R caused a significant reduction of RUNX1 activity in this assay (**Figure 2B and S1B**). A previously reported dominant-negative variant p.R204Q was used as a reference (24, 25). Notably, p.K117* and p.S141fs proteins were only modestly expressed compared to WT and other variants, suggesting that the lack of RUNX1 activity may be due to reduced translation and/or the instability of truncated protein. To further characterize these *RUNX1* variants in a more relevant cellular context, we engineered the Jurkat T-ALL cell line in which each *RUNX1* variant of interest was individually inserted into the safe harbor *AAVS1* locus (**Figure S2**)(26) and a GFP tag was added to the C-terminus of RUNX1 target gene *GZMA(27)* (**Figure 2C and S3**). Using this model system, RUNX1 transactivation activity could be directly measured as the GFP intensity in *RUNX1* variants knock-in cells, in the presence of endogenous *RUNX1* (**Figure 2D**). As shown in **Figure 2E**, the introduction of WT *RUNX1* as well as most missense variants (p.N153Y, p.T246M, p.A329T, p.P359R, and p.M418V) led to robust GFP signals relative to cells with no *RUNX1* insertion at the AAVS locus (EV), confirming WT like transcription activator activity. By contrast, cells with K117* and S141fs showed no expression of variant RUNX1 protein and thus only baseline GFP signals (**Figure 2E and S1C**). Insertion of the p.Q213fs, p.R232fs, p.Y287*, and p.G365R variants resulted in the lowest GFP intensity (despite robust protein expression) (**Figure 2E and S1C**), suggesting these variants not only lost their transcription activator activity but also repressed endogenous RUNX1 in a plausibly dominant-negative manner. We next analyzed subcellular localization and CBFβ cofactor interaction of deleterious variants that are readily expressed, including p.Q213fs, p.R232fs, p.Y287*, and p.G365R (**Figure S4**). Fluorescence microscopy of HEK293T cells ectopically expressing *RUNX1* variants showed that

p.Q213fs, p.R232fs, p.Y287*, and p.G365R proteins mostly remained in the nucleus and retained the ability to interact with CBFβ (**Figure 3**).

**Effects of *RUNX1* variants on the differentiation and proliferation of human cord blood CD34+ cells *in vitro***

We sought to examine the effects of *RUNX1* variants on hematopoietic differentiation *in vitro* using human cord blood CD34+ cell as the model system. Because p.K117* and p.S141fs resulted in complete loss of function with no dominant negative effects, we chose not to further characterize them. For the remaining deleterious variants, we selected p.R232fs, p.Y287* and p.G365R to represent frameshift, nonsense, and missense variants, respectively. *RUNX1* variants were ectopically expressed in human CD34+ cells which were then subjected to differentiation, proliferation, and apoptosis assays *in vitro* (**Figure 4A-C**).

In colony formation assays conditioned for erythroid and myeloid progenitor cell growth, the expression of p.R232fs, p.Y287*, and p.G365R significantly repressed burst-forming unit erythroid (BFU-E) and increased colony-forming unit granulocyte-macrophage (CFU-GM) colonies compared to CD34+ cells transduced with WT RUNX1 (**Figure 4D and S5A-B**). The immunophenotype of these progenitor cells was confirmed by flow cytometry (**Figure S6A**), with cell identities also examined using Giemsa staining (**Figure S5C**). plating, *RUNX1* variants (especially p.Y287*) gave rise to more CFU-GM colonies relative to WT, suggesting their potential effects on hematopoietic cells self-renewal (**Figure 4E**). Long-term culture showed that the *RUNX1* variant-transduced CD34+ cells proliferated significantly faster with concomitant reduction in apoptosis, compared to WT *RUNX1* cells (**Figure 4F-G and S6B**).

With culture conditions for megakaryocyte differentiation, expression of *RUNX1* variants consistently resulted in a significant reduction of CD41a+/CD42b+ population compared to WT (**Figure 4H**). These variants also repressed the generation of CD5+/CD7+ T cells from the CD34+

population (**Figure 4I**). Collectively, these results suggested that *RUNX1* variants promoted myeloid differentiation while repressing megakaryocyte and T cell differentiation *in vitro*.

### ***RUNX1* variants have highly distinctive patterns of DNA binding and are associated with altered post-translational modifications**

To understand the molecular effects of *RUNX1* variants, we comprehensively profiled RUNX1 binding across the genome using chromatin immunoprecipitation-sequencing (ChIP-seq). We first engineered three isogenic Jurkat cell lines in which each *RUNX1* variant (p.R232fs, p.Y287*, and p.G365R) was individually knocked-in at the endogenous locus in a hemizygous fashion to represent heterozygous genotype seen in patients (**Figure 5A and 5B**). In these models, we introduced the HA and TY1 epitope tags at the 3' end of the coding exon on the variant and WT *RUNX1* alleles, respectively (**Figure S7-S10 and Figure 5C**). This enabled us to separately profile variant or WT RUNX1 binding using HA or TY1 antibodies (**Figure 5D**). To control for differences in ChIP-seq efficiency between HA and TY1 antibodies, we also generate Jurkat cells in which WT *RUNX1* alleles were tagged with HA or TY1 respectively (**Figure S9 and S10**).

ChIP-seq showed both similarities and differences in RUNX1 binding between variant and WT proteins in T-ALL genome (**Figure 5E-F**). Calculating a pair-wise Pearson correlation coefficient in ChIP-seq signal intensity at all identified binding sites, we observed the highest concordance between WT and p.G365R and also between p.Y287X and p.R232fs (**Figure 5F and S11**). By contrast, the truncating variants showed a very distinct pattern of RUNX1 binding compared to missense variant or WT (**Figure 5F and S11**). For each RUNX1 variant, we also identified binding sites unique to variant protein vs those shared with WT RUNX1 (**Figure S12A**). In total, we defined 59,151 peaks shared by WT and variant RUNX1, and 2,026, 782, 93 ChIP-seq signals specific to p.R232fs, p.Y287*, and p.G365R, respectively. While WT RUNX1 binding sites were found both within and outside of promoter regions, variant-specific sites were almost exclusively

in introns and intergenic regions (**Figure S12B**). Our RUNX1 ChIP-seq results were generally consistent with results published previously in hematopoietic tissues(27, 28) (**Table S1**).

In T-ALL, RUNX1 often functions through a transcription factor complex with multiple components (e.g., GATA3, TAL1, E2A, HEB, and LMO1)(27), a question arises as to whether or how this might be affected by RUNX1 variants. Comparing with previously published ChIP-seq data of RUNX1 complex members(27), we noted that WT RUNX1 binding sites overlap with GATA3, TAL1, E2A, HEB, and LMO1 binding, but they were largely absent within ChIP-seq peaks unique to RUNX1 variants, with the exception of CTCF(29) (**Figure S12C**). This was further confirmed by de novo motif analyses (**Table S2**). Furthermore, we performed gene set enrichment analysis to identify pathways that were preferentially affected by RUNX1 variants and observed a preponderance of IL2-STAT5 and TGFβ-signaling genes (**Figure S12D**). At last, we identified 402, 424, and 136 differentially expressed genes between p.R232fs, p.Y287*, and p.G365R and WT RUNX1 Jurkat cells by RNA-seq, respectively, most of which also harbor RUNX1 binding sites as identified by ChIP-seq (**Figure S12E and Tables S3-S5**).

Interestingly, the p.G365R variant gave rise to a novel methylation site in RUNX1, with mono- or di-methylation of the arginine residue confirmed by mass spectrometry and Western blot analysis (**Figure 5G and 5H**). Immunoprecipitation–mass spectrometry results suggested that RUNX1 protein methylation at this site may disrupt its interaction with TUBB family proteins (TUBB2A, TUBB2B, TUBB4B, TUBB5, TUB8, *et al.*) and heat shock proteins, but with an increase of CBFβ binding (**Table S6**).

**Somatic genomic abnormalities in T-ALL with germline *RUNX1* variants**

To characterize the somatic genomic landscape of T-ALL with germline *RUNX1* variants, we analyzed whole genome seq of six cases with p.K117*, p.S141fs, p.Q213fs, p.R232fs, p.Y287*, and p.G365R variants, which were contrasted with 263 T-ALL with somatic mutations in *RUNX1* or WT genotype (30). Five of six T-ALL (83.3%) with germline *RUNX1* variants had a somatic

*JAK3* mutation, significantly higher compared to the frequency of *JAK3* mutation percentage in T-ALL cases without germline variants in *RUNX1* (7.6%, p-value = $2.59 \times 10^{-5}$) (30) or T-ALL cases with somatic mutations in *RUNX1* (27.3%, p-value = 0.05) (**Figure 6A**). *JAK3* mutations in T-ALL c ases with germline *RUNX1* variants were located in either the pseudo-kinase domain (M511I and R657Q) or in the kinase domain (L950V, **Figure S13 and Tables S7 and S8**). Of interest, the patient with a germline *RUNX1*-p.R232fs variant also subsequently acquired a somatic *RUNX1* mutation (R169_E5splice_region). Mutation signature analyses showed highly significant enrichment of the SBS1, SBS5, SBS8, SBS9, and SBS18 patterns (COSMIC Mutational signatures V3, synapse.org ID: syn12009743) (31) (**Figure S14**) in *RUNX1* variant T-ALL samples. This is of interest because SBS5 was previously associated with the process of hematopoietic cell divisions and one of the main contributors to mutagenesis during T-ALL evolution (32).

We also performed RNA-seq of T-ALL with germline *RUNX1* variants and compared the expression profile with cases with germline *RUNX1* variants (p.S141fs, p.R232fs, p.Y287*, and p.G365R), somatic *RUNX1* mutations, or WT *RUNX1* (N = 4, 11 and 252, respectively). Based on hierarchical clustering of global expression profile, *RUNX1*-variant cases (either germline or somatic) consistently clustered with T-ALL with early T-cell precursor immunophenotype (ETP) or near-ETP cases (**Figure 6B and Table S9**). These results are consistent with previous reports of the preponderance of *RUNX1* variants in ETP T-ALL (33).

### ***RUNX1* and *JAK3* mutation induced ETP T-ALL in mice**

To model *RUNX1*-related T-ALL leukemogenesis, especially in conjunction with somatic *JAK3* mutation, we introduced different combinations of *RUNX1* and *JAK3* mutations ($RUNX1^{R232fs}$ and $JAK3^{M511I}$) into mouse hematopoietic progenitor cells ($Lin^-/Sca\text{-}1^+/C\text{-}Kit^+$) and monitored leukemia development *in vivo* after transplantation. We hereafter refer to recipient mice with LSK cells transduced with empty vector, $RUNX1^{R232fs}$, $JAK3^{M511I}$, and $JAK3^{M511I}/RUNX1^{R232fs}$ as "control",

"*RUNX1*$^{M}$", "*JAK3*$^{M}$", and "*JAK3*$^{M}$*RUNX1*$^{M}$" mice, respectively. At 4 months, peripheral leukocyte counts of *JAK3*$^{M}$ and *JAK3*$^{M}$*RUNX1*$^{M}$ mice (41.78 ± 44.3 × $10^3$ cells/μL and 14.93 ± 3.42 × $10^3$ cells/μL respectively) were significantly higher than control mice (8.84 ± 2.00 × $10^3$ cells/μL), and the lowest peripheral leukocyte counts were seen in *RUNX1*$^{M}$ mice (6.10 ± 2.03 × $10^3$ cells/μL, **Figure 7A**). Flow cytometry analysis at this time point showed a significant increase of CD8+ T cells in *JAK3*$^{M}$ mice (**Figure 7B-C**), compared with control mice. By contrast, *JAK3*$^{M}$*RUNX1*$^{M}$ mice showed an increase in Mac1+ population and lower T cell population, suggesting an outgrowth of cells with ETP immunophenotype (**Figure 7B-C**).

At 6 to 10 months after transplantation, both *JAK3*$^{M}$*RUNX1*$^{M}$ and *JAK3*$^{M}$ mice developed overt leukemia presented with leukocytosis and splenomegaly, with a penetrance of 66.7% and 100%, respectively (**Figure 7D-F and S15**). The thymus of *JAK3*$^{M}$*RUNX1*$^{M}$ mice showed a significantly increase of CD4-CD8- (DN) T cells, particularly DN1 cells, as compared with *JAK3*$^{M}$ mice (**Figure 7G-H**). Circulating leukemic cells of *JAK3*$^{M}$*RUNX1*$^{M}$ mice showed a markedly higher Mac1+ population, but lower lymphoid surface marker as compared with *JAK3*$^{M}$ mice (**Figure 7I**). Also, flow analysis of spleen and bone marrow showed a similar leukemia immunophenotype as peripheral blood (**Figure 7I**). These results indicate that *JAK3*$^{M}$*RUNX1*$^{M}$ induced the ETP-ALL phenotype *in vivo*. There was also a trend for higher Mac1+ cells with lower level of CD3+ cells in the peripheral blood of *RUNX1*$^{M}$ mice but they never developed leukemia within this timeframe (**Figure 7A**).

## Discussion

RUNX1 plays significant roles in definitive hematopoiesis by regulating the differentiation of myeloid, megakaryocyte, and lymphoid lineages. In this study, we comprehensively investigated *RUNX1* variation in ALL patients and identified highly deleterious germline variants in T-ALL, most of which were frameshift or nonsense variations. By multilayer functional experiments and comprehensive epigenomic and genomic profiling analyses, we systematically characterized *RUNX1* variant function and identified *JAK3* mutations as the predominant cooperating somatic lesions in T-ALL. Furthermore, *RUNX1* variant, in conjunction with mutant *JAK3*, directly gave rise to ETP T-ALL *in vivo*. These findings advance our understanding of the role of *RUNX1* in the predisposition to childhood ALL.

*RUNX1* is one of the most frequent target genes of chromosomal translocation, mutation, and copy number alteration in different hematopoietic diseases and leukemia. *RUNX1* germline variants are associated with FPDMM (OMIM #601399) (15, 16, 18, 34). Although most patients with FPD progress to myeloid malignancies, ALL has been reported in a minority of cases (16, 17). In MDS and AML with germline *RUNX1* variants, somatic *RUNX1* mutations are the most common acquired genomic alteration, suggesting that they are key cooperating events for leukemia progression (22, 35). Other studies identified somatic mutations in *CDC25C*, *GATA2*, *BCOR*, *PHF6*, *JAK2*, *DNMT3A*, *TET*, *ASXL1,* albeit with lower frequencies. (22, 35, 36). By contrast, we identified *JAK3* mutations as the predominant co-occurring event with *RUNX1* germline variants in T-ALL, which consistently drove an ETP phenotype in patients and in mouse models in T-ALL. Therefore, we postulate that while germline *RUNX1* variants disrupt normal hematopoiesis and generally increase the risk of leukemia, the lineage specification of these hematological malignancies is mostly dictated by secondary mutations acquired later in life.

Activating *JAK3* mutations have been reported in T-ALL (33). *In vivo* studies using a murine bone marrow transplantation model showed that *JAK3* mutations in the pseudo-kinase domain caused T-cell lymphoproliferative disease that progressed to T-ALL, mainly by increasing the CD8+ cell

population (37, 38). This is in line with our observation that *JAK3*$^{M}$ mice exhibited a significant accumulation of CD8+ cells in thymus, peripheral blood, spleen, and bone marrow. However, *JAK3*$^{M}$*RUNX1*$^{M}$ mouse developed lymphoid leukemia with a distinctive phenotype which recapitulated human ETP T-ALL features and is similar to previously reported mouse models (*e.g.,* circulating leukemic cells expressed the myeloid cell marker Mac1, but not the lymphoid markers CD8/CD3)(39, 40). Also, the CD4-CD8- (DN), especially DN1 population was particularly enriched in thymocytes from *JAK3*$^{M}$*RUNX1*$^{M}$ mice, as compared with *JAK3*$^{M}$ mice. Alongside genomic findings in T-ALL patients, these *in vivo* experiments indicate that *RUNX1* dominant-negative variants plus *JAK3*-activating mutations most likely result in the ETP T-ALL. The segregation of *RUNX1* variants with ETP T-ALL is of interest because historically this subtype is associated with inferior treatment outcomes (41). However, the survival gap between ETP vs other T-ALL is no longer significant with contemporary treatment regimens. For these reasons, children with ETP T-ALL are not routinely taken to allogeneic transplantation. Currently, there are insufficient data to inform the treatment of patients with ETP-ALL who harbor germline *RUNX1* variations. In theory, these children remain at risk for persistent thrombocytopenia and development of second AML and/or MDS. Allogeneic hematopoietic transplantation using a *RUNX1* WT donor could potentially cure both of these problems. That said, decisions regarding allogeneic transplantation are complex and must take into account the condition and age of the patient, donor availability, and preferences of the patient, treating physicians and transplant specialists.

A recent study by Brown et al. comprehensively described the genomic landscape of *RUNX1*-related FPD and myeloid malignancy from 130 families (22). In this cohort, missense and truncating germline *RUNX1* variants were equally represented. While truncating variants occurred in both the RHD and the TAD domains, missense variants were largely restricted to the former. This pattern is significantly different from that in the lymphoid malignancies as described here. In T-ALL, deleterious *RUNX1* variants were predominantly nonsense or frameshift and the only missense variant resided in the activation domain. Unfortunately, we do not have family history

for children with T-ALL carrying *RUNX1* germline variants, and therefore cannot ascertain the exact penetrance on leukemia or FPD. However, given the profound effects on RUNX1 activity and a range of phenotypes *in vitro* and *in vivo*, these variants are defined as likely pathogenic according to the American College of Medical Genetics (ACMG) classification (**Table 1 and Table S10**). In fact, the p.Y287* variant seen in our T-ALL cohort has been previously linked to FPD, and functional characterization indicated that this variant causes defective megakaryocyte differentiation in the iPSC model (42). In B-ALL, almost all variants were missense and localized outside of the RHD domain. Although these variants showed little effect on RUNX1 transcriptional activity level, some of them were predicted to be damaging variants by REVEL (43)(**Table 1**). More comprehensive functional assays might be needed to definitively determine the effects of these variants. Finally, we found that RUNX1 variants dramatically alter the colony formation of BFU-E and CFU-GM, in a pattern similar to that seen with *GATA2* mutation (44). *GATA2* (or *GATA1*) expression was not influenced by *RUNX1* variants in our human CD34+ cell models (data not shown). However, GATA2 can co-localize on chromatin with RUNX1 (45), and these factors plausibly cooperate with each other to regulate hematopoietic differentiation.

Genome-wide patterns of RUNX1 binding have been investigated extensively using ChIP-seq assays (27, 46, 47), but there is a paucity of studies directly examining target genes of variant RUNX1. When this was attempted in the past, variant RUNX1 was either ectopically expressed in iPSC or cord blood CD34+ cells, raising the possibility of false positives due to artificially high levels of RUNX1(48). This is also hindered by the lack of antibodies that specifically recognize WT but not variant RUNX1. To overcome these issues, we engineered Jurkat cells with heterozygous knock-in of *RUNX1* variants (p.R232fs/WT, p.Y287*/WT, and p.G365R/WT) using the CHASE-KI method (49). In this model, we also introduced the HA and TY1 epitope tags at the 3' end of the coding exon on the variant and WT *RUNX1* allele, respectively. Our model recapitulated *RUNX1* variant status in patients with T-ALL and enabled us to profile variant or WT RUNX1 binding using different antibodies. Moreover, our ChIP-seq result indicated that the C-

terminal truncating variants p.R232fs and p.Y287* variants indeed exhibited a distinct binding pattern than the full-length p.G365R variant and WT RUNX1.

Although our studies comprehensively characterized *RUNX1* variant functions using a variety of orthogonal methods, our model systems and assays were not without limitations. For example, ectopic expression of *RUNX1* variant can artificially increase gene activity that is not seen under physiological conditions, and this can be problematic for studying loss-of-function variants when endogenous *RUNX1* is also present. We tried to mitigate these issues by including WT *RUNX1* as control and our assays indeed confirmed the effects of known pathogenic variants (**Figure 2A, B, and E**, p.R204Q). Non-hematopoietic cells such as HEK293T and HeLa have been used extensively to study RUNX1 function (24, 50, 51), but one could easily argue against their tissue relevance in the context of RUNX1-related leukemia, which is why we performed extensive experiments to confirm *RUNX1* function in T-ALL cell lines and also in human cord blood CD34+ cells. Recent development of gene editing techniques in induced pluripotent stem cell (iPSC) provides an exciting system for this type of work (42, 52). For example, CRISPR-Cas9 gRNA mediated homology-directed repair (HDR) or base editing in iPSC system can precisely introduce *RUNX1* variant at the endogenous locus and in the presence of WT allele, and the hematopoietic differentiation potential of these engineered progenitor cells can be directly characterized *in vitro*.

In summary, we comprehensively described *RUNX1* germline variants in childhood ALL. Using multiple functional assays, we identified highly deleterious germline variants in T-ALL and their biochemical and cellular effects. In addition, we characterized somatic genomic alterations associated with *RUNX1* germline variation in T-ALL, illustrating the interplay between acquired and inherited genetic variants in the context of leukemia pathogenesis.

## Methods

### Patients

A total of 6,190 ALL cases were included for *RUNX1* targeted sequencing: 4,132 children with newly diagnosed B-ALL enrolled on the Children's Oncology Group (COG) AALL0232 (n = 2,224), P9904/5/6 (n = 1,634), and AALL0331 (n = 274) protocols; 704 children with newly diagnosed B-ALL enrolled on the St.Jude Total XIII and XV protocols; 1,231 children with newly diagnosed T-ALL enrolled on the COG AALL0434 protocols; and 123 children with newly diagnosed T-ALL enrolled on the St. Jude Total XIII and XV protocols (**Figure 1A**) (53-56). Family histories were not available for patients on the COG studies. Peripheral blood or bone marrow from children with ALL during remission was collected as a source of genomic DNA. Due to the leukemia-free status of these samples, we consider them as “germline like” and the variants identified in these samples are provisionally of germline origin.

For targeted *RUNX1* sequencing in the ALL cohort, Illumina dual-indexed libraries were created from the germline DNA of 6,190 children, and pooled in sets of 96 before hybridization with customized Roche NimbleGene SeqCap EZ probes (Roche, Roche NimbleGen, Madison, WI, USA) to capture the *RUNX1* genomic region. Quantitative PCR was used to define the appropriate capture product titer necessary to efficiently populate an Illumina HiSeq 2000 flowcell for paired-end 2x100 bp sequencing. Coverage of at least 20-fold depth was achieved across the targeted *RUNX1* locus for 99.2% of samples. Sequence reads in FASTQ format were mapped and aligned using the Burrows-Wheeler Aligner (BWA)(57, 58), and genetic variants were called using the GATK pipeline (version 3.1)(58), as previously described, and annotated using the ANNOVAR program(59) with the annotation databases including GRCh37/hg19, GRCh38/hg38 RefSeq(60), and REVEL (43). Variant classification was done following the ACMG guidelines (61). Non-coding, and synonymous coding variants were excluded from further consideration for this study.

### Genomic Analysis of Patient Samples

Whole-genome sequencing and RNA sequencing were performed for T-ALL cases with germline RUNX1 variants, whenever available samples were identified. Whole genome seq was done for matched germline and leukemia samples, whereas RNA-seq was done only for leukemia samples. Briefly, DNA was purified using the QIAamp DNA Blood Mini Kit (Qiagen, 51104), and RNA was purified using the RiboPure RNA Purification Kit (Thermo Fisher Scientific, AM1928). DNA (250-1000 ng) and RNA (500-1000 ng) was sent to St. Jude Hartwell center for sequencing.

Details for functional experiments, leukemia modeling in mouse, genomic analyses, and other experiments can be found in supplemental file.

**Data access**

ChIP-seq and RNA-seq data have been submitted to the National Center for Biotechnology Information (NCBI) Gene Expression Omnibus under accession no. GSE178239. Whole genome seq data are available through the European Genome-Phenome Archive (EGA-box-1704).

**Statistics**

Statistical analyses were performed using Student t-test, Dunnett's test, G-test, or Fisher's exact test. Multiple comparisons were accounted for using Dunnett's test for analysis when applicable. The choice of statistical test was based on data distribution, as noted in Figure legends. All tests were two-tailed. Statistical significance was defined as $p < 0.05$ and displayed as *($p < 0.05$), ** ($p < 0.01$), *** ($p < 0.001$), or ns (not significant).

**Study approval**

Human subject research was approved by Institutional Review Boards at St. Jude and COG affiliated institutions and informed consent was obtained from parents, guardians, or patients, and assent from patients, as appropriate. All animal experiments were conducted according to the protocols approved by the St. Jude Institutional Animal Care and Use Committee.

More detailed methods can be found in supplemental files.

## Author contributions

JJY initiated and led the project; JJY and YL designed the functional experiments; YL, XZ, RZ performed in vitro experiments; CL and YL designed CRISPR/Cas9 experiment; YL performed in vivo experiments; WY analysis the genomic data; CK performed ACMG annotation; MD, SSW, KPD, JMG, EAR, WLC, KRR, CGM, WEE, CHP, SPH, DTT, MRR, MLL contributed to the data gathering; JJY, WY, MQ, CHP, SPH, RH, KEN, CGM, and MLC interpreted the data. PPL, TS, KEN provided relevant intellectual input and edited the manuscript. JY and YL wrote the manuscript. All the authors reviewed and commented on the manuscript.

**Acknowledgments**

We thank the Hartwell Center for Bioinformatics and Biotechnology, the Flow Cytometry and Cell Sorting Core, the Cytogenetic Shared Resource, the Animal Research Center of St. Jude Children's Research Hospital for their technical support in performing experiments included in this study. This work was supported in part by P50GM115279, R01CA241452, P30CA21765.

## References


1. Iacobucci I, and Mullighan CG. Genetic Basis of Acute Lymphoblastic Leukemia. *J Clin Oncol.* 2017;35(9):975-83.
2. Churchman ML, Qian M, Te Kronnie G, Zhang R, Yang W, Zhang H, et al. Germline Genetic IKZF1 Variation and Predisposition to Childhood Acute Lymphoblastic Leukemia. *Cancer Cell.* 2018;33(5):937-48 e8.
3. Trevino LR, Yang W, French D, Hunger SP, Carroll WL, Devidas M, et al. Germline genomic variants associated with childhood acute lymphoblastic leukemia. *Nat Genet.* 2009;41(9):1001-5.
4. Xu H, Zhang H, Yang W, Yadav R, Morrison AC, Qian M, et al. Inherited coding variants at the CDKN2A locus influence susceptibility to acute lymphoblastic leukaemia in children. *Nat Commun.* 2015;6:7553.
5. Perez-Andreu V, Roberts KG, Harvey RC, Yang W, Cheng C, Pei D, et al. Inherited GATA3 variants are associated with Ph-like childhood acute lymphoblastic leukemia and risk of relapse. *Nat Genet.* 2013;45(12):1494-8.
6. Perez-Andreu V, Roberts KG, Xu H, Smith C, Zhang H, Yang W, et al. A genome-wide association study of susceptibility to acute lymphoblastic leukemia in adolescents and young adults. *Blood.* 2015;125(4):680-6.
7. Papaemmanuil E, Hosking FJ, Vijayakrishnan J, Price A, Olver B, Sheridan E, et al. Loci on 7p12.2, 10q21.2 and 14q11.2 are associated with risk of childhood acute lymphoblastic leukemia. *Nat Genet.* 2009;41(9):1006-10.
8. Migliorini G, Fiege B, Hosking FJ, Ma Y, Kumar R, Sherborne AL, et al. Variation at 10p12.2 and 10p14 influences risk of childhood B-cell acute lymphoblastic leukemia and phenotype. *Blood.* 2013;122(19):3298-307.

9. Lee SHR, Qian M, Yang W, Diedrich JD, Raetz E, Yang W, et al. Genome-wide association study of susceptibility loci for TCF3-PBX1 acute lymphoblastic leukemia in children. *J Natl Cancer Inst.* 2020.

10. Qian M, Cao X, Devidas M, Yang W, Cheng C, Dai Y, et al. TP53 Germline Variations Influence the Predisposition and Prognosis of B-Cell Acute Lymphoblastic Leukemia in Children. *J Clin Oncol.* 2018;36(6):591-9.

11. Moriyama T, Metzger ML, Wu G, Nishii R, Qian M, Devidas M, et al. Germline genetic variation in ETV6 and risk of childhood acute lymphoblastic leukaemia: a systematic genetic study. *Lancet Oncol.* 2015;16(16):1659-66.

12. Wang Q, Stacy T, Binder M, Marin-Padilla M, Sharpe AH, and Speck NA. Disruption of the Cbfa2 gene causes necrosis and hemorrhaging in the central nervous system and blocks definitive hematopoiesis. *Proc Natl Acad Sci U S A.* 1996;93(8):3444-9.

13. Huang G, Shigesada K, Ito K, Wee HJ, Yokomizo T, and Ito Y. Dimerization with PEBP2beta protects RUNX1/AML1 from ubiquitin-proteasome-mediated degradation. *EMBO J.* 2001;20(4):723-33.

14. Kanno T, Kanno Y, Chen LF, Ogawa E, Kim WY, and Ito Y. Intrinsic transcriptional activation-inhibition domains of the polyomavirus enhancer binding protein 2/core binding factor alpha subunit revealed in the presence of the beta subunit. *Mol Cell Biol.* 1998;18(5):2444-54.

15. Owen CJ, Toze CL, Koochin A, Forrest DL, Smith CA, Stevens JM, et al. Five new pedigrees with inherited RUNX1 mutations causing familial platelet disorder with propensity to myeloid malignancy. *Blood.* 2008;112(12):4639-45.

16. Preudhomme C, Renneville A, Bourdon V, Philippe N, Roche-Lestienne C, Boissel N, et al. High frequency of RUNX1 biallelic alteration in acute myeloid leukemia secondary to familial platelet disorder. *Blood.* 2009;113(22):5583-7.

17. Nishimoto N, Imai Y, Ueda K, Nakagawa M, Shinohara A, Ichikawa M, et al. T cell acute lymphoblastic leukemia arising from familial platelet disorder. *Int J Hematol.* 2010;92(1):194-7.
18. Song WJ, Sullivan MG, Legare RD, Hutchings S, Tan X, Kufrin D, et al. Haploinsufficiency of CBFA2 causes familial thrombocytopenia with propensity to develop acute myelogenous leukaemia. *Nat Genet.* 1999;23(2):166-75.
19. Grossmann V, Kern W, Harbich S, Alpermann T, Jeromin S, Schnittger S, et al. Prognostic relevance of RUNX1 mutations in T-cell acute lymphoblastic leukemia. *Haematologica.* 2011;96(12):1874-7.
20. Della Gatta G, Palomero T, Perez-Garcia A, Ambesi-Impiombato A, Bansal M, Carpenter ZW, et al. Reverse engineering of TLX oncogenic transcriptional networks identifies RUNX1 as tumor suppressor in T-ALL. *Nat Med.* 2012;18(3):436-40.
21. Quentin S, Cuccuini W, Ceccaldi R, Nibourel O, Pondarre C, Pages MP, et al. Myelodysplasia and leukemia of Fanconi anemia are associated with a specific pattern of genomic abnormalities that includes cryptic RUNX1/AML1 lesions. *Blood.* 2011;117(15):e161-70.
22. Brown AL, Arts P, Carmichael CL, Babic M, Dobbins J, Chong CE, et al. RUNX1-mutated families show phenotype heterogeneity and a somatic mutation profile unique to germline predisposed AML. *Blood Adv.* 2020;4(6):1131-44.
23. Huang G, Zhang P, Hirai H, Elf S, Yan X, Chen Z, et al. PU.1 is a major downstream target of AML1 (RUNX1) in adult mouse hematopoiesis. *Nat Genet.* 2008;40(1):51-60.
24. Harada H, Harada Y, Tanaka H, Kimura A, and Inaba T. Implications of somatic mutations in the AML1 gene in radiation-associated and therapy-related myelodysplastic syndrome/acute myeloid leukemia. *Blood.* 2003;101(2):673-80.

25. Osato M, Asou N, Abdalla E, Hoshino K, Yamasaki H, Okubo T, et al. Biallelic and heterozygous point mutations in the runt domain of the AML1/PEBP2alphaB gene associated with myeloblastic leukemias. *Blood.* 1999;93(6):1817-24.

26. Matreyek KA, Stephany JJ, and Fowler DM. A platform for functional assessment of large variant libraries in mammalian cells. *Nucleic Acids Res.* 2017;45(11):e102.

27. Sanda T, Lawton LN, Barrasa MI, Fan ZP, Kohlhammer H, Gutierrez A, et al. Core transcriptional regulatory circuit controlled by the TAL1 complex in human T cell acute lymphoblastic leukemia. *Cancer Cell.* 2012;22(2):209-21.

28. Beck D, Thoms JA, Perera D, Schutte J, Unnikrishnan A, Knezevic K, et al. Genome-wide analysis of transcriptional regulators in human HSPCs reveals a densely interconnected network of coding and noncoding genes. *Blood.* 2013;122(14):e12-22.

29. Cuddapah S, Jothi R, Schones DE, Roh TY, Cui K, and Zhao K. Global analysis of the insulator binding protein CTCF in chromatin barrier regions reveals demarcation of active and repressive domains. *Genome Res.* 2009;19(1):24-32.

30. Liu Y, Easton J, Shao Y, Maciaszek J, Wang Z, Wilkinson MR, et al. The genomic landscape of pediatric and young adult T-lineage acute lymphoblastic leukemia. *Nat Genet.* 2017;49(8):1211-8.

31. Bamford S, Dawson E, Forbes S, Clements J, Pettett R, Dogan A, et al. The COSMIC (Catalogue of Somatic Mutations in Cancer) database and website. *Br J Cancer.* 2004;91(2):355-8.

32. Sentis I, Gonzalez S, Genesca E, Garcia-Hernandez V, Muinos F, Gonzalez C, et al. The evolution of relapse of adult T cell acute lymphoblastic leukemia. *Genome Biol.* 2020;21(1):284.

33. Zhang J, Ding L, Holmfeldt L, Wu G, Heatley SL, Payne-Turner D, et al. The genetic basis of early T-cell precursor acute lymphoblastic leukaemia. *Nature.* 2012;481(7380):157-63.

34. Michaud J, Wu F, Osato M, Cottles GM, Yanagida M, Asou N, et al. In vitro analyses of known and novel RUNX1/AML1 mutations in dominant familial platelet disorder with predisposition to acute myelogenous leukemia: implications for mechanisms of pathogenesis. *Blood.* 2002;99(4):1364-72.

35. Antony-Debre I, Duployez N, Bucci M, Geffroy S, Micol JB, Renneville A, et al. Somatic mutations associated with leukemic progression of familial platelet disorder with predisposition to acute myeloid leukemia. *Leukemia.* 2016;30(4):999-1002.

36. Yoshimi A, Toya T, Kawazu M, Ueno T, Tsukamoto A, Iizuka H, et al. Recurrent CDC25C mutations drive malignant transformation in FPD/AML. *Nat Commun.* 2014;5:4770.

37. Degryse S, de Bock CE, Cox L, Demeyer S, Gielen O, Mentens N, et al. JAK3 mutants transform hematopoietic cells through JAK1 activation, causing T-cell acute lymphoblastic leukemia in a mouse model. *Blood.* 2014;124(20):3092-100.

38. Cornejo MG, Kharas MG, Werneck MB, Le Bras S, Moore SA, Ball B, et al. Constitutive JAK3 activation induces lymphoproliferative syndromes in murine bone marrow transplantation models. *Blood.* 2009;113(12):2746-54.

39. Booth CAG, Barkas N, Neo WH, Boukarabila H, Soilleux EJ, Giotopoulos G, et al. Ezh2 and Runx1 Mutations Collaborate to Initiate Lympho-Myeloid Leukemia in Early Thymic Progenitors. *Cancer Cell.* 2018;33(2):274-91 e8.

40. Wang C, Oshima M, Sato D, Matsui H, Kubota S, Aoyama K, et al. Ezh2 loss propagates hypermethylation at T cell differentiation-regulating genes to promote leukemic transformation. *J Clin Invest.* 2018;128(9):3872-86.

41. Teachey DT, and O'Connor D. How I treat newly diagnosed T-cell acute lymphoblastic leukemia and T-cell lymphoblastic lymphoma in children. *Blood.* 2020;135(3):159-66.

42. Connelly JP, Kwon EM, Gao Y, Trivedi NS, Elkahloun AG, Horwitz MS, et al. Targeted correction of RUNX1 mutation in FPD patient-specific induced pluripotent stem cells rescues megakaryopoietic defects. *Blood.* 2014;124(12):1926-30.
43. Ioannidis NM, Rothstein JH, Pejaver V, Middha S, McDonnell SK, Baheti S, et al. REVEL: An Ensemble Method for Predicting the Pathogenicity of Rare Missense Variants. *Am J Hum Genet.* 2016;99(4):877-85.
44. Katsumura KR, Mehta C, Hewitt KJ, Soukup AA, Fraga de Andrade I, Ranheim EA, et al. Human leukemia mutations corrupt but do not abrogate GATA-2 function. *Proc Natl Acad Sci U S A.* 2018;115(43):E10109-E18.
45. Chacon D, Beck D, Perera D, Wong JW, and Pimanda JE. BloodChIP: a database of comparative genome-wide transcription factor binding profiles in human blood cells. *Nucleic Acids Res.* 2014;42(Database issue):D172-7.
46. Giambra V, Jenkins CR, Wang H, Lam SH, Shevchuk OO, Nemirovsky O, et al. NOTCH1 promotes T cell leukemia-initiating activity by RUNX-mediated regulation of PKC-theta and reactive oxygen species. *Nat Med.* 2012;18(11):1693-8.
47. Wilkinson AC, Ballabio E, Geng H, North P, Tapia M, Kerry J, et al. RUNX1 is a key target in t(4;11) leukemias that contributes to gene activation through an AF4-MLL complex interaction. *Cell Rep.* 2013;3(1):116-27.
48. Gerritsen M, Yi G, Tijchon E, Kuster J, Schuringa JJ, Martens JHA, et al. RUNX1 mutations enhance self-renewal and block granulocytic differentiation in human in vitro models and primary AMLs. *Blood Adv.* 2019;3(3):320-32.
49. Hyle J, Zhang Y, Wright S, Xu B, Shao Y, Easton J, et al. Acute depletion of CTCF directly affects MYC regulation through loss of enhancer-promoter looping. *Nucleic Acids Res.* 2019;47(13):6699-713.

50. Decker M, Lammens T, Ferster A, Erlacher M, Yoshimi A, Niemeyer CM, et al. Functional classification of RUNX1 variants in familial platelet disorder with associated myeloid malignancies. *Leukemia.* 2021.

51. Imai Y, Kurokawa M, Izutsu K, Hangaishi A, Takeuchi K, Maki K, et al. Mutations of the AML1 gene in myelodysplastic syndrome and their functional implications in leukemogenesis. *Blood.* 2000;96(9):3154-60.

52. Estevez B, Borst S, Jarocha DJ, Sudunagunta VS, Gonzalez M, Garifallou J, et al. RUNX1 haploinsufficiency causes a marked deficiency of megakaryocyte-biased hematopoietic progenitor cells. *Blood.* 2021.

53. Larsen EC, Devidas M, Chen S, Salzer WL, Raetz EA, Loh ML, et al. Dexamethasone and High-Dose Methotrexate Improve Outcome for Children and Young Adults With High-Risk B-Acute Lymphoblastic Leukemia: A Report From Children's Oncology Group Study AALL0232. *J Clin Oncol.* 2016;34(20):2380-8.

54. Bowman WP, Larsen EL, Devidas M, Linda SB, Blach L, Carroll AJ, et al. Augmented therapy improves outcome for pediatric high risk acute lymphocytic leukemia: results of Children's Oncology Group trial P9906. *Pediatr Blood Cancer.* 2011;57(4):569-77.

55. Pui CH, Sandlund JT, Pei D, Campana D, Rivera GK, Ribeiro RC, et al. Improved outcome for children with acute lymphoblastic leukemia: results of Total Therapy Study XIIIB at St Jude Children's Research Hospital. *Blood.* 2004;104(9):2690-6.

56. Pui CH, Relling MV, Sandlund JT, Downing JR, Campana D, and Evans WE. Rationale and design of Total Therapy Study XV for newly diagnosed childhood acute lymphoblastic leukemia. *Ann Hematol.* 2004;83 Suppl 1:S124-6.

57. Li H, and Durbin R. Fast and accurate short read alignment with Burrows-Wheeler transform. *Bioinformatics.* 2009;25(14):1754-60.

588 58. McKenna A, Hanna M, Banks E, Sivachenko A, Cibulskis K, Kernytsky A, et al. The
589 Genome Analysis Toolkit: a MapReduce framework for analyzing next-generation DNA
590 sequencing data. *Genome Res.* 2010;20(9):1297-303.
591 59. Wang K, Li M, and Hakonarson H. ANNOVAR: functional annotation of genetic variants
592 from high-throughput sequencing data. *Nucleic Acids Res.* 2010;38(16):e164.
593 60. Pruitt KD, Brown GR, Hiatt SM, Thibaud-Nissen F, Astashyn A, Ermolaeva O, et al.
594 RefSeq: an update on mammalian reference sequences. *Nucleic Acids Res.*
595 2014;42(Database issue):D756-63.
596 61. Richards S, Aziz N, Bale S, Bick D, Das S, Gastier-Foster J, et al. Standards and
597 guidelines for the interpretation of sequence variants: a joint consensus recommendation
598 of the American College of Medical Genetics and Genomics and the Association for
599 Molecular Pathology. *Genet Med.* 2015;17(5):405-24.
600

## Figures and figure legends

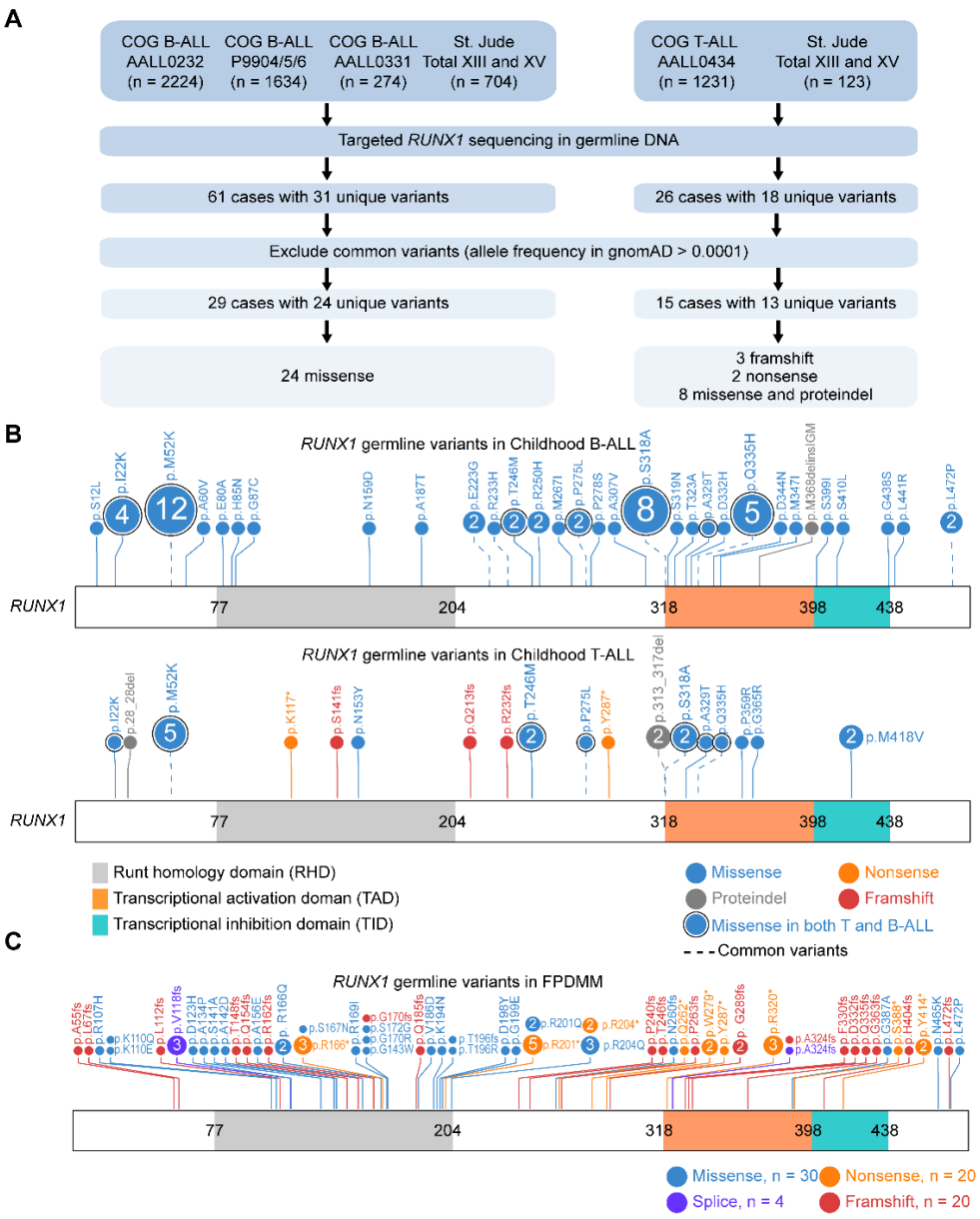


**Figure 1. Germline *RUNX1* variants in childhood B- and T-ALL.** (A) CONSORT diagram of the Children's Oncology Group (COG) and St. Jude Children's Research Hospital (St. Jude) patients included in this study. (B) Protein domain plot of RUNX1 and the amino acid substitutions predicted to result from the germline *RUNX1* variants identified in this study. The upper panel showed germline *RUNX1* variants in B-ALL cases, and the lower panel showed those in T-ALL cases. The numbers in the circles indicate the number of cases in our cohort that harbor the variant of interest. (C) Protein domain plot of RUNX1 and the germline RUNX1 variants identified previously in FPDMM. Data were retrieved from recently published paper (22).

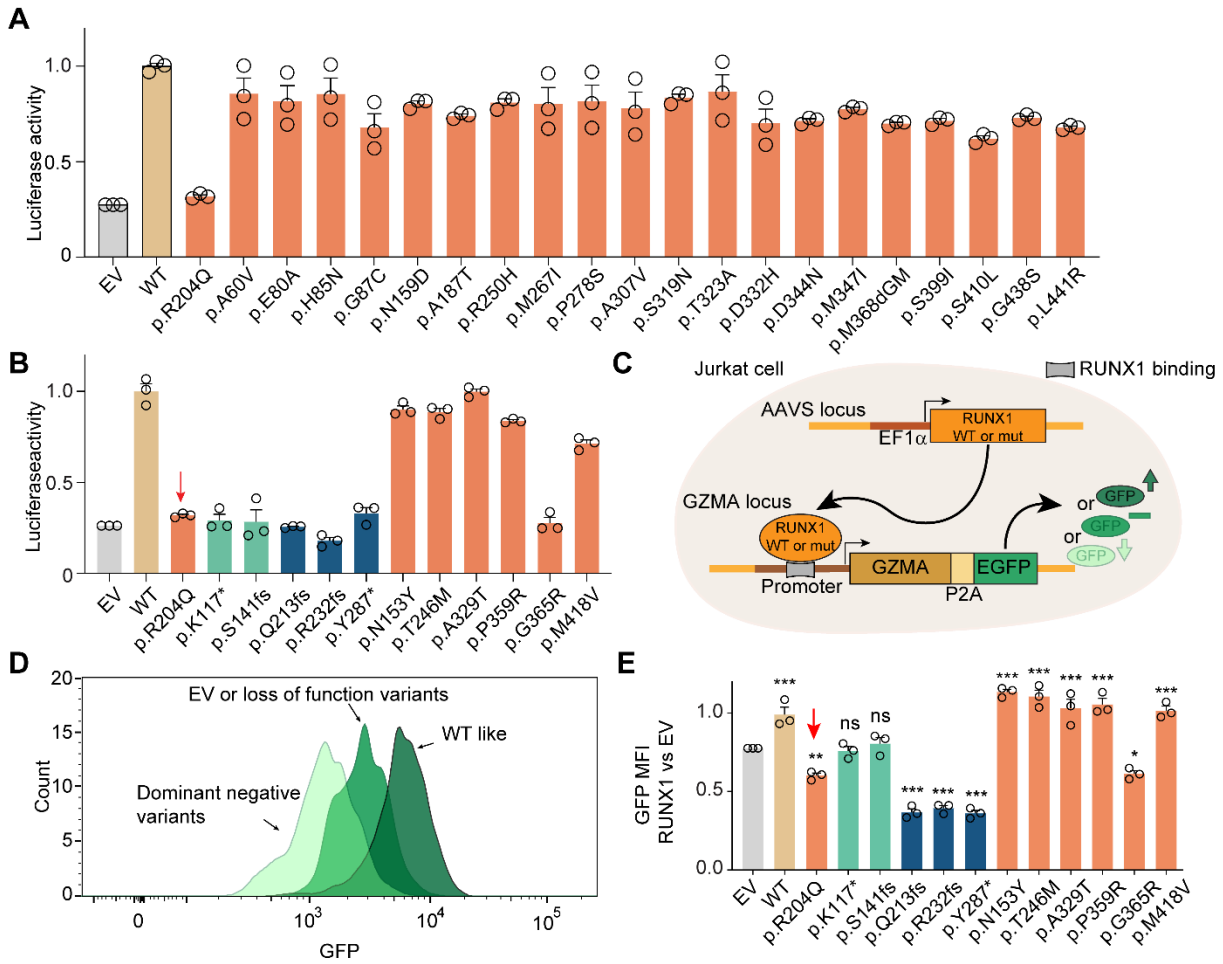


**Figure 2. Germline *RUNX1* variants influence transcription factor activity, subcellular localization, and CBFβ interaction.** (A-B) Luciferase reporter gene assay (driven by the *PU.1* promoter in Hela cells) showed minimal effects on transcription factor activity by missense *RUNX1* variants identified in B-ALL (A) and T-ALL (B). A previously reported damaging variant p.R204Q was included as the reference for luciferase assay (red arrow). (C) Design of the Jurkat landing-pad system to measure RUNX1 variant activity in T-ALL. *RUNX1* (either WT or variant) was inserted at the AAVS locus. EGFP coding sequence was knocked at the 3'-end of *GZMA*, a RUNX1 target gene. RUNX1 transcription factor activity was determined by flow cytometry of GFP signal which reflects RUNX1-driven *GZMA* transcription. (D) Flow cytometry analysis of Jurkat cells expressing different *RUNX1* variants. Cells harboring dominant-negative, loss of function, and WT-like RUNX1 variants exhibited the lowest, moderate, and highest GFP signals, respectively. (E) The GFP signal from Jurkat cells expressing each *RUNX1* variant (relative to WT) is shown in bar graph. Data represent mean ± SEM (n = 3). The difference of each variant relative to EV was evaluated using Dunnett's test. p.R204Q was used as control.

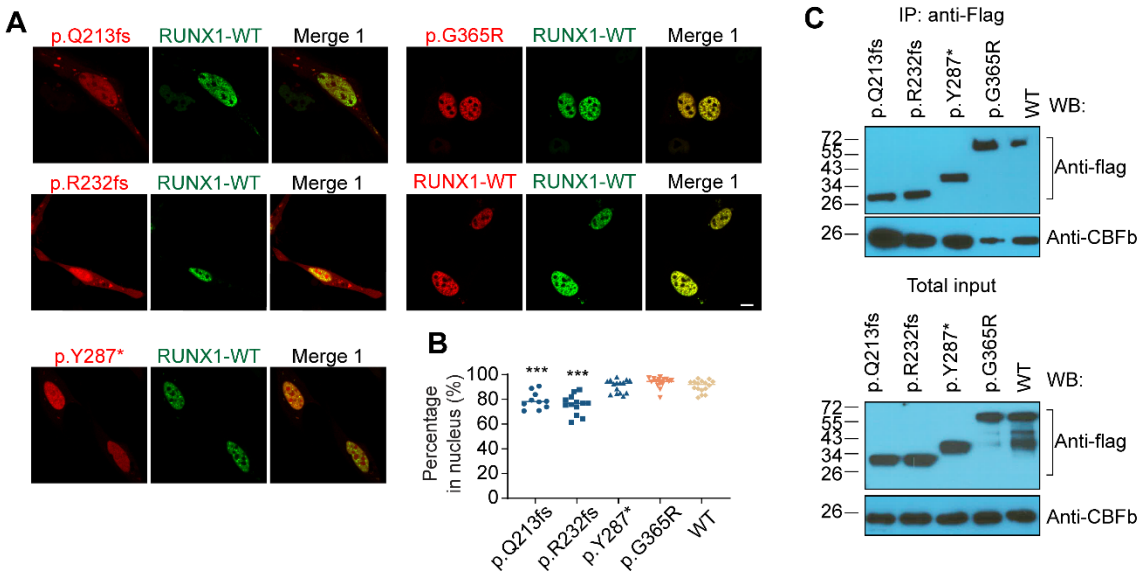


**Figure 3. Dominant negative *RUNX1* variants retain nuclear localization and CBFβ interaction.** (A) Immunofluorescence microscopy shows subcellular localization of mCherry-tagged variant proteins and EGFP-tagged WT RUNX1. Variant and WT RUNX1 were fused to mCherry and EGFP and expressed transiently in HEK293T cells, which were then subjected to imaging analyses. Scale bar = 10 μm. (B) Summary of the percentage of mCherry signals in nucleus are shown as dot plot. The difference of each variant relateive to WT was evaluated using Dunnett's test. p.Q213fs: n=10; p.R232fs: n=13; p.Y287*: n=15; p.G365R: n=16; WT: n=16. (C) Co-immunoprecipitation assay was performed to determine RUNX1-CBFβ interaction for each deleterious variant. Experiments were performed in HEK293T cells. RUNX1 proteins were pulled down using anti-FLAG-M2 beads and the presence or absence of CBFβ in the pellet was examined by immunoblotting.

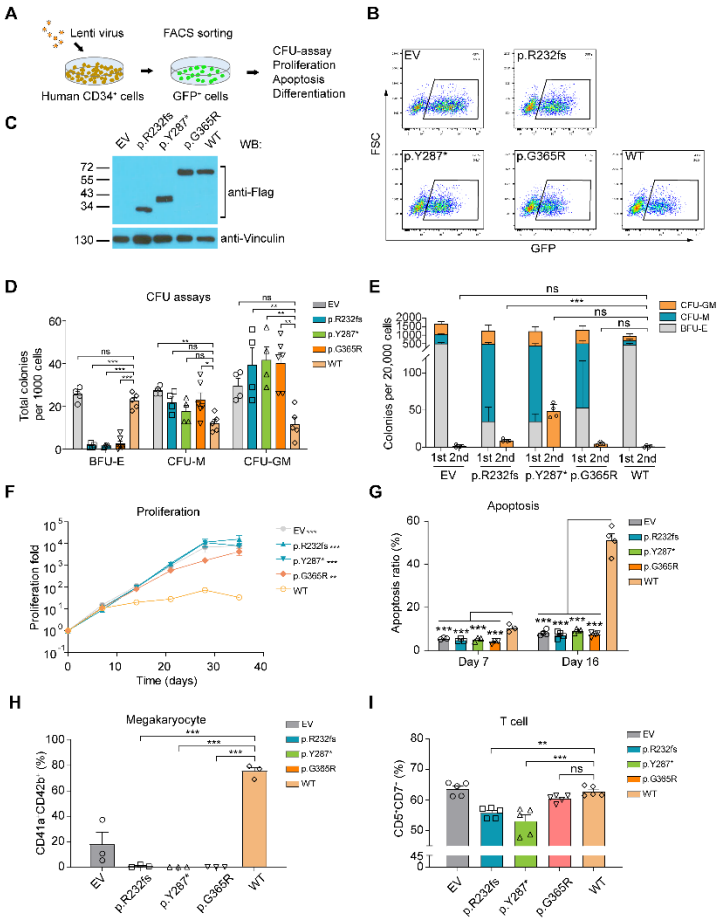


**Figure 4. *RUNX1* variants affect in vitro differentiation of human cord blood CD34+ cells.** (A-B) Schematic description of the *in vitro* hematopoietic differentiation assay. *RUNX1* variants (with IRES-GFP) were lentivirally introduced into human cord blood CD34+ cells. Successfully transduced cells were sorted by flow cytometry (B) and processed for colony forming unit assays, and assessed for cell proliferation and apoptosis, as appropriate. (C) Western blot was used to confirm RUNX1 expression, with vinculin as the internal control. (D) One thousand RUNX1-expressing CD34+ cells were plated in MethoCult H4034. The Y-axis shows the count of colonies for each lineage: burst-forming unit erythroid (BFU-E), colony-forming unit-macrophage (CFU-M), and colony-forming unit granulocyte-macrophage (CFU-GM). EV, p.R232fs, and p.Y287*: n = 3; p.G365R: n = 6; WT: n = 5. (E) Colony number of CFU-assays and CFU-replating assays (n = 4). (F) Proliferation of RUNX1-expressing CD34+ cells were monitored for 5 weeks, in Iscove's Modified Dulbecco Medium (IMDM) medium containing 20% BIT9500, 10 ng/mL FLT-3 ligand, TPO, SCF, IL-3, and IL-6. The number of cells was counted every week for 5 weeks. N = 4. (G) Apoptosis of RUNX1-transduced CD34+ cells after 7 (n = 3) and 16 (n = 4) days of culture (same culture medium as F) was measured by flow cytometry using Annexin-V and DAPI antibodies. (H-I) CD34+ cells ectopically expressing RUNX1 variants were also subjected to in vitro differentiation assays for megakaryocyte (n = 3) or T (n = 4) cell lineages. Following RUNX1 transduction, cells were cultured in the presence of SFEMII containing megakaryocyte expansion supplement or T-Cell progenitor differentiation supplement for 2 weeks. Megakaryocyte (H) was identified as CD41a+/CD42b+, and T cells (I) were defined as CD5+/CD7+ by flow cytometry. Data represent mean ± SEM. P-value were estimated by using Dunnett's test.

Figure 4

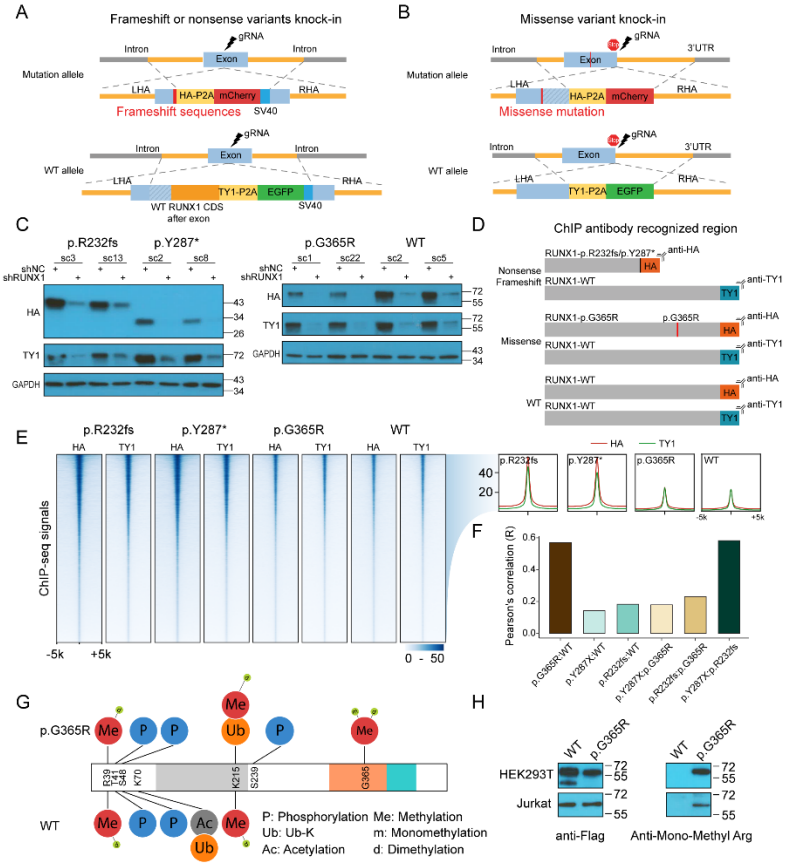


**Figure 5. *RUNX1* variants are associated with distinctive DNA binding patterns and altered post-translational modifications.** (A-B) Schematic representation of Jurkat cell models for RUNX1 ChIP-seq profiling. p.R232fs, p.Y287*, and p.G365R were knocked-in using CRISPR-cas9 at the endogenous locus in a heterozygous fashion. TY1 and HA epitopes were inserted to the coding sequence of WT and variant RUNX1, respectively. This design enables ChIP-seq of each protein simultaneously using two different antibodies. Detailed information can be found in Figure S7-S9. Sequence of the HDR templates are provided as Supplemental Data. (C) Immunoblot confirmed that the expression of HA- and TY1-tagged RUNX1, and the identity of these bands were verified using *RUNX1* shRNA. (D) Schematic representation of ChIP-seq strategy. To control for the difference in ChIP efficiency using HA vs. TY1 antibodies, we also included Jurkat cells with each copy of the WT RUNX1 tagged with HA and TY1, respectively. (E) Heatmap shows the ChIP-seq signals of variants and WT RUNX1 in Jurkat cells (left panel). Each row represents a genomic locus centered around the summit of the ChIP-seq peak, with the color indicating the signal intensity. The aggregation plot (right panel) showed the average of ChIP-seq signal intensity for all peaks identified with the HA-tagged (red line) vs. TY1-tagged RUNX1 proteins (green line). (F) Across all ChIP-seq peaks identified, we derived HA/TY1 signal ratio to quantify variant RUNX1 binding normalized against WT proteins. Comparing this ratio at each peak between different variants and also with WT, we calculated Pearson's correlation of each pair to indicate the overall similarity in RUNX1 binding pattern. (G) Immunoprecipitation–Mass Spectrometry assays identified p.G365R-specific arginine methylation at this residue in HEK293T cells. (H) p.G365R methylation was confirmed by immunoblotting using an anti-Mono-Methyl Arginine antibody in both HEK293T and Jurkat cells.

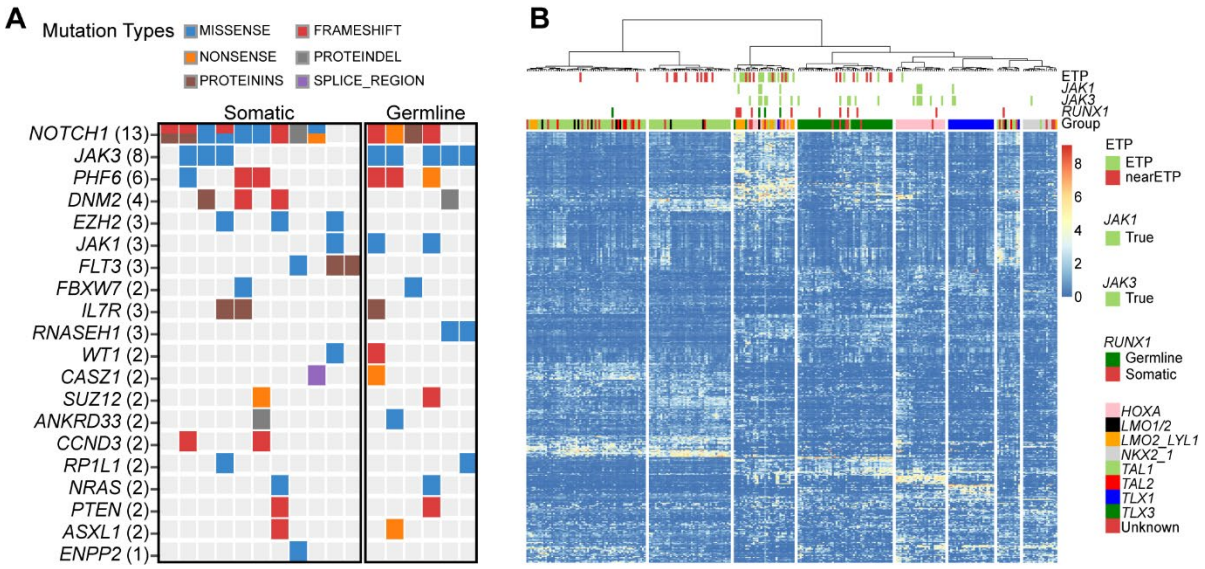


**Figure 6. Somatic *JAK3* mutations co-occur in T-ALL with germline deleterious *RUNX1* variants.** (A) Somatic *JAK3* mutations were significantly enriched in T-ALL cases with germline *RUNX1* variants. Whole genome seq of remission samples for 17 T-ALL cases, 6 and 11 with germline variants or somatic mutations in *RUNX1*, respectively. (B) RNA-seq was analyzed for 267 T-ALL cases, including 252, 4, and 11 subjects with WT RUNX1, carrying germline variants or somatic mutations in this gene. Unsupervised clustering shows that RUNX1-variant cases, either germline or somatic, clustered tightly with T-ALL with ETP and near-ETP immunophenotypes.

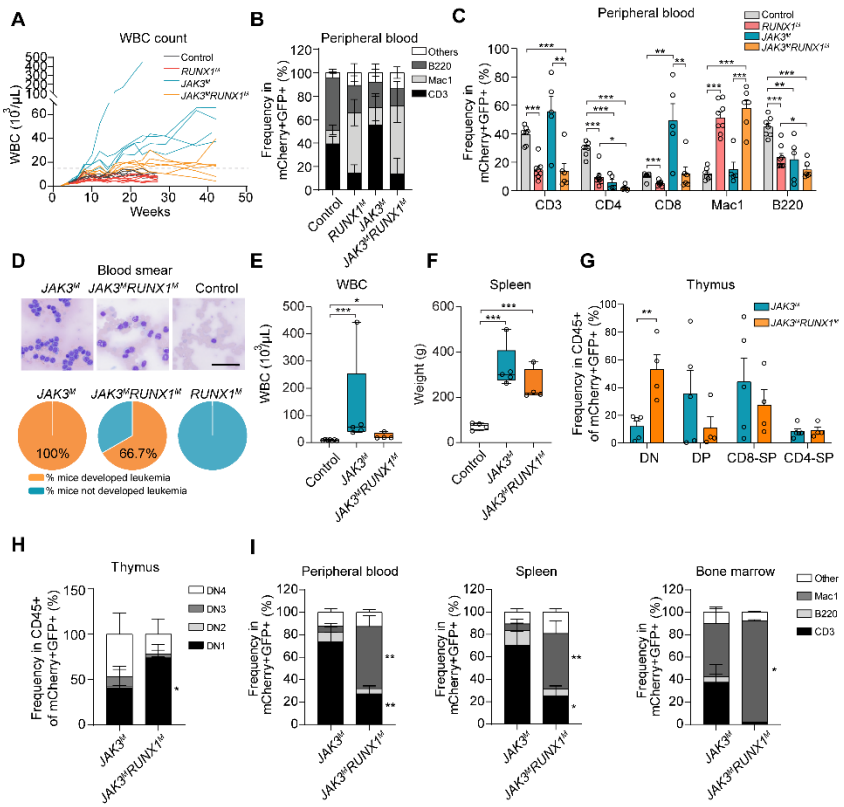


**Figure 7. *RUNX1* variation and *JAK3* mutation jointly drive ETP phenotype in murine bone marrow transplantation model.** (A) Peripheral leukocyte count of *RUNX1*$^{M}$, *JAK3*$^{M}$, *JAK3*$^{M}$*RUNX1*$^{M}$, and control mice. Mice hematopoietic stem and progenitor cells were lentivirally transduced with *RUNX1*$^{M}$ *and JAK3*$^{M}$ constructs or empty vector, and injected into recipient 8 weeks old female mice. Peripheral blood count was monitored biweekly. (B-C) There was a significant increase in the CD8+ population in *JAK3*$^{M}$ mice than in control mice. *RUNX1*$^{M}$ and *JAK3*$^{M}$*RUNX1*$^{M}$ mice showed increases of Mac1+ cells and fewer CD3+ cells than control or *JAK3*$^{M}$ mice at 4 months. N=7, 8, 5, 6 for control, *RUNX1*$^{M}$, *JAK3*$^{M}$, and *JAK3*$^{M}$*RUNX1*$^{M}$, respectively. (D) Upper panel: blood smear of *JAK3*$^{M}$ and *JAK3*$^{M}$*RUNX1*$^{M}$ mice at the time of sacrifice, and control mice at 4 months. Scale bar=50 μm. Lower panel: the percentage of mice developed leukemia in each group. *JAK3*$^{M}$: 100%; *JAK3*$^{M}$*RUNX1*$^{M}$: 66.7%. (E) Peripheral leukocyte count of *JAK3*$^{M}$*RUNX1*$^{M}$ (n=4) and *JAK3*$^{M}$ (n=5) at the time of sacrifice, and control (n=7) mice after 4 months of transplantation. (F) Spleen weight of *JAK3*$^{M}$ (n=5) and *JAK3*$^{M}$*RUNX1*$^{M}$ (n=4) mice at the time of sacrifice and control mice (n=4) after 4 months of transplantation. (G and H) Thymocyte immunophenotype of *JAK3*$^{M}$ (n=5) and *JAK3*$^{M}$*RUNX1*$^{M}$ (n=4) mice at the time of sacrifice. Co-expression of *RUNX1*$^{M}$ and *JAK3*$^{M}$ resulted in a drastic increase in DN1 population compared with mice receiving LSK cells expressing JAK3$^{M}$ only. (I) In peripheral blood (n=3), bone marrow (n=4), and spleen (n=4), *JAK3*$^{M}$*RUNX1*$^{M}$ mice showed a significant increase in Mac1+ population and a reduction of the CD3+ population compared to *JAK3*$^{M}$ (n=5) mice. For E and F, p-value was estimated by using Dunnett's test. For B, C, G, H, I, data represent mean ± SEM, p-value was generated by t-test.

715 **Table1. Germline RUNX1 Variants in Pediatric ALL Cases**

| Protein (NM_001754) | CDS (NM_001754) | ExonicFunc.refGene | ALL Subtype (the number of cases) | Allele frequence in gnomAD (Allele count) | REVEL score | ACMG classification |
|---|---|---|---|---|---|---|
| p.S12L | c.C35T | missense | B-ALL (1) | (7.95E-06) 2 | 0.305 | VUS |
| p.I22K | c.T65A | missense | B-ALL (4) and T-ALL (1) | (1.99E-04) 56 | 0.271 | LB |
| p.28_28del | c.82_84del | nonframeshift_deletion | T-ALL (1) | (4.62E-05) 13 | . | VUS |
| p.M52K | c.T155A | missense | B-ALL (12) and T-ALL (5) | (2.46E-04) 65 | 0.845 | VUS |
| p.A60V | c.C179T | missense | B-ALL (1) | (7.40E-05) 17 | 0.284 | B |
| p.E80A | c.A239C | missense | B-ALL (1) | (1.22E-05) 3 | 0.856 | VUS |
| p.H85N | c.C253A | missense | B-ALL (1) | (3.59E-05) 10 | 0.852 | LB |
| p.G87C | c.G259T | missense | B-ALL (1) | . | 0.918 | VUS |
| p.K117X | c.A349T | stopgain | T-ALL (1) | . | . | LP |
| p.S141fs | c.422_423insAACC | frameshift_insertion | T-ALL (1) | . | . | LP |
| p.N153Y | c.A457T | missense | T-ALL (1) | . | 0.956 | VUS |
| p.N159D | c.A475G | missense | B-ALL (1) | . | 0.956 | VUS |
| p.A187T | c.G559A | missense | B-ALL (1) | (3.98E-06) 1 | 0.96 | VUS |
| p.Q213fs | c.637delC | frameshift_deletion | T-ALL (1) | . | . | LP |
| p.E223G | c.A668G | missense | B-ALL (2) | (1.24E-04) 31 | 0.799 | VUS |
| p.R232fs | c.696delG | frameshift_deletion | T-ALL (1) | . | . | LP |
| p.R233H | c.G698A | missense | B-ALL (1) | (1.67E-04) 47 | 0.514 | LB |
| p.T246M | c.C737T | missense | B-ALL (2) and T-ALL (2) | (4.61E-05) 13 | 0.4 | VUS |
| p.R250H | c.G749A | missense | B-ALL (2) | (3.91E-05) 11 | 0.488 | VUS |
| p.M267I | c.G801A | missense | B-ALL (1) | (3.93E-05) 11 | 0.283 | VUS |
| p.P275L | c.C824T | missense | B-ALL (2) and T-ALL (1) | (2.03E-04) 51 | 0.146 | B |
| p.P278S | c.C832T | missense | B-ALL (1) | (1.19E-05) 3 | 0.275 | VUS |
| p.Y287X | c.C861G | stopgain | T-ALL (1) | . | . | LP |
| p.A307V | c.C920T | missense | B-ALL (1) | . | 0.098 | VUS |
| p.313_317del | c.939_950del | nonframeshift_deletion | T-ALL (2) | (1.73E-04) 49 | . | LB |
| p.S318A | c.T952G | missense | B-ALL (8) and T-ALL (2) | (8.13E-04) 230 | 0.093 | B |
| p.S319N | c.G956A | missense | B-ALL (1) | | 0.127 | VUS |

| | | | | | | |
|---|---|---|---|---|---|---|
| p.T323A | c.A967G | missense | B-ALL (1) | (1.59E-05) 4 | 0.063 | LB |
| p.A329T | c.G985A | missense | B-ALL (1) and T-ALL (1) | . | 0.067 | LB |
| p.D332H | c.G994C | missense | B-ALL (1) | . | 0.391 | VUS |
| p.Q335H | c.G1005T | missense | B-ALL (5) and T-ALL (1) | (1.70E-04) 43 | 0.4 | B |
| p.D344N | c.G1030A | missense | B-ALL (1) | (6.20E-05) 16 | 0.082 | LB |
| p.M347I | c.G1041A | missense | B-ALL (1) | (8.79E-06) 2 | 0.374 | VUS |
| p.P359R | c.C1076G | missense | T-ALL (1) | . | 0.62 | VUS |
| p.G365R | c.G1093C | missense | T-ALL (1) | . | 0.776 | LP |
| p.M368delinsIGM | c.1103_1104insCGGCAT | nonframeshift_insertion | B-ALL (1) | (7.34E-05) 17 | . | VUS |
| p.S399I | c.G1196T | missense | B-ALL (1) | (2.89E-05) 5 | 0.116 | VUS |
| p.S410L | c.C1229T | missense | B-ALL (1) | (1.56E-05) 3 | 0.339 | VUS |
| p.M418V | c.A1252G | missense | T-ALL (2) | (9.79E-05) 3 | 0.14 | LB |
| p.G438S | c.G1312A | missense | B-ALL (1) | . | 0.23 | VUS |
| p.L441R | c.T1322G | missense | B-ALL (1) | (7.28E-06) 1 | 0.74 | VUS |
| p.L472P | c.T1415C | missense | B-ALL (2) | (1.99E-04) 23 | 0.414 | B |

Additional variant annotation (e.g., chromosomal position) can be found in Table S10.